Vimentin promotes actin assembly by stabilizing ATP-actin subunits at the barbed end.

Lilian Paty[a], Maritzaida Varela-Salgado[a], Quang D. Tran[a,b], Antoine Jégou[a*], Guillaume Romet-Lemonne[a*], and Cécile Leduc[a*]

[a]Université Paris Cité, CNRS, Institut Jacques Monod, F-75013 Paris, France

[b]Present address: Department of Physiology and Biomedical Engineering, Mayo Clinic, Rochester, MN 55905, USA

[*] corresponding authors:

Email: antoine.jegou@ijm.fr; romet@ijm.fr; cecile.leduc@ijm.fr

Author Contributions: LP, AJ, GRL and CL designed the research; LP, MVS, QT, CL performed experiments; LP analyzed the data; LP and CL wrote the manuscript with input from all the co-authors; CL supervised the project.

Competing Interest Statement: The authors declare no competing interests.

Classification: Biophysics

Keywords: cytoskeleton, intermediate filaments, assembly dynamics, cytoskeletal crosstalk, in vitro reconstitution

Abstract

Vimentin intermediate filaments play essential roles in maintaining cell integrity and regulating numerous cellular functions. In particular, vimentin cooperates with the actin cytoskeleton in key cellular processes that rely on actin dynamics, such as such as migration, division, and mechanosensing. While there is evidence that these two cytoskeletal components interact in cells, the underlying molecular mechanisms are only partially understood. Actin and vimentin can interact through biochemical signaling pathways or via cross-linkers, but whether they engage in a direct protein-protein interaction has remained controversial, in part because such interactions are difficult to isolate and characterize in cells. Using in vitro reconstitution and total internal reflection fluorescence microscopy to monitor the elongation of single actin filaments, we show that vimentin promotes actin elongation at the barbed end in a dose-dependent manner. Neither the vimentin tail nor head domains are required for this effect, and both filamentous and non-filamentous vimentin enhance actin elongation. We find that this acceleration results from a stabilization of actin subunits at the barbed end. Strikingly, this effect depends on the nucleotide state of actin, as the acceleration is only observed for the elongation from ATP-actin, and not ADP-actin monomers. This stabilization also enables vimentin to promote the nucleation of actin filaments. Consistently, magnetic pull-down assays demonstrate a direct, albeit weak, interaction between vimentin and actin monomers. Altogether, these findings identify vimentin as an unexpected new actor in the regulation of actin dynamics at the barbed end and bring new insights into the functional role of vimentin through cytoskeletal crosstalk.

Introduction

The cytoskeleton is a dynamic network of three interconnected filament systems: actin, microtubules, and intermediate filaments, that allow cells to shape and organize themselves in space and time while

mechanically engaging with their environment. Intermediate filaments are composed of a large family of proteins whose expression levels are cell- and tissue-type specific (1–4). Among them, vimentin is expressed in mesenchymal cells and widely used as a marker of the epithelial-to-mesenchymal transition, during which epithelial cells acquire migratory and invasive properties (5, 6). Unlike actin and microtubules, which rapidly remodel through active turnover, vimentin self-assembles into long-lived apolar filaments (3, 7–9), yet is involved in highly dynamic processes such as migration, division, and mechanosensing (4, 10–13). Growing evidence suggests that vimentin contributes to these functions through its crosstalk with the other cytoskeletal filaments (2, 14–16), including actin (17). Early studies showed that vimentin-deficient cells exhibit reduced acto-myosin contractility (12). More recent work revealed that vimentin coordinates actin stress fiber assembly (18–20), orients traction forces that drive migration (21), and tunes cell stress by assisting in actomyosin-based force transmission (10). There is also a mechanical synergy between the two types of filaments (22), which is crucial for maintaining cell integrity (23). The actin-vimentin interplay likely relies on reciprocal regulation of filament organization and dynamics, with vimentin modulating actin in both non-dividing (18, 24–26) and dividing cells (11, 13) and actin in turn influencing vimentin (18, 27–29). This interplay is mediated through indirect biochemical signaling, direct interactions, or interactions via crosslinkers (2, 14, 18, 30–33), but the precise molecular mechanisms remain to be fully elucidated.

In vitro reconstitution with purified proteins provides a powerful approach to dissect how actin and vimentin coordinate their activities, as it can disentangle their interactions from the complexity of the cellular environment. Bulk rheology studies of actin–vimentin networks have suggested that the observed viscoelastic properties of the composite networks cannot be explained without direct actin-vimentin interactions (34, 35), and that vimentin's tail domain is implicated in the interaction (34). However, another study has argued that the mechanics of composite networks could be explained solely by the additive properties of their individual components, without requiring direct filament–filament binding (36). More recently, single-filament imaging found no evidence for actin-vimentin filament co-alignment, suggesting that if there is an interaction between the filaments, it must be transient and weak (37). Thus, whether actin and vimentin filaments interact directly, and how such interactions might influence filament dynamics, remains unresolved. Understanding the effect of vimentin on actin filaments alone in simplified in vitro systems is necessary, before adding more components, such as crosslinkers and regulatory proteins, in more complex bottom-up approaches that would come closer to the cellular context.

Here, using an actin single-filament assay, we found that vimentin directly promotes actin filament nucleation and elongation, despite its weak affinity for actin. We show that the molecular mechanism responsible for the enhanced elongation involves vimentin stabilizing actin subunits at the barbed end in a nucleotide state-dependent manner. These findings reveal a previously unrecognized role for vimentin as a regulator of actin filament growth, highlighting a direct interaction through which vimentin intermediate filaments can influence actin dynamics.

Results

Vimentin promotes actin filament elongation at the barbed end

In order to assess the impact of vimentin on actin assembly dynamics, we used an assay that allows direct visualization of actin elongation at the single filament level using time-lapse Total Internal Reflection Fluorescence (TIRF) microscopy, hereinafter referred to as "actin polymerization assay" (Fig. 1A). Small pre-polymerized biotinylated fragments of actin filaments (F-actin) (Fig. 1A, magenta) were first anchored to a passivated glass surface coated with neutravidin. Upon addition of 0.5 µM of actin monomers in the ATP-bound state (ATP-G-actin, 10% fluorescently labeled), with a low fraction of biotinylation (~0.15%), filaments elongated at their fast-growing barbed-end with sparse anchoring points along their length (~0.5 anchors per µm) (Fig. 1A, yellow). At this actin concentration, the elongation of the pointed end is negligible over the time scale of the experiments. This low biotinylation

level minimized potential effects on elongation while maintaining sufficient proximity to the surface for automated filament tracking. Actin filament elongation was monitored in either assembly buffer alone (control) or buffer containing pre-assembled vimentin filaments at 1 mg/mL (18 µM vimentin monomers). As depicted in Fig. 1B, F-actin elongated faster in the presence of vimentin filaments (bottom) than in the control condition (top). Automated filament tracking and systematic quantification of the elongation rate (Fig. 1C) confirmed that this effect was consistently reproducible across repeated experiments (N = 11 independent replicates) (Fig. 1D), and robust with salinity (Fig. S1). Control experiments verified that the actin elongation rates with low biotinylation were comparable to those without anchoring points, using methylcellulose to confine the filaments (Fig. S2A). Moreover, we verified that vimentin's effect on actin elongation was similar in both anchoring and methylcellulose conditions (Fig. S2B). However, because methylcellulose induces actin-vimentin co-alignment (potentially bundling them through depletion effects), as observed when a small fraction of vimentin was fluorescently labeled within the network (Fig. S2C), we rather used sparse anchoring to confine the filaments on the surface. Because, in cells, actin monomers are bound to profilin and F-actin elongate from profilin-G-actin complexes, we verified that vimentin also promoted elongation from profilin-G-actin (Fig. S3). These results demonstrate that the sole presence of vimentin filaments is sufficient to accelerate actin elongation in the absence of any actin-vimentin crosslinkers.

Non-filamentous vimentin also promotes actin elongation

We next asked whether vimentin's effect on actin elongation depends on vimentin's filament-forming capacity. In vimentin-expressing cells, vimentin is found as elongated filaments, short filaments also called squiggles, and tetramers (4, 38, 39). At low ionic strength, purified vimentin spontaneously self-assembles into tetramers (3, 40). By raising the ionic strength, tetramers associate laterally into short filaments known as unit-length filaments (ULFs), which subsequently anneal end-to-end to form longer filaments (3, 40). To arrest assembly at different stages, we produced different mutants of vimentin (Fig. 2A). The headless mutant ($Vim^{\Delta head}$), which lacks the N-terminal disordered head domain, forms tetramers but fails to laterally assemble into ULFs (40). The point-mutated vimentin Vim^{Y117L} forms ULFs that cannot anneal end-to-end to form longer filaments (41). Performing the actin polymerization assay (Fig. 1A) with these vimentin mutants revealed the same increase in actin elongation rate as observed with wild-type vimentin (Vim^{WT}), compared with the vimentin-free control condition (Fig. 2B). We conclude that the effect of vimentin on actin elongation can occur even with vimentin tetramers, and does not require vimentin to be assembled into long filaments.

Vimentin's disordered tail domain is not required to promote actin elongation

Because vimentin's disordered tail domain has been proposed to mediate a direct actin-vimentin interaction (34), we asked whether this domain is required for the acceleration of actin assembly. To address this question, we produced a truncated version of vimentin lacking the last 55 amino acids ($Vim^{\Delta tail}$) and performed the actin polymerization assay (Fig. 1A) in the presence of this mutant. This tailless vimentin mutant assembles into filaments (3, 40). $Vim^{\Delta tail}$ increased the actin elongation rate to the same extent as wild-type vimentin, with no significant difference between the two conditions (Fig. 2C), indicating that the tail domain is not required to promote actin elongation at the barbed end.

Vimentin promotes actin elongation in a dose-dependent manner

Since vimentin subunits alone are sufficient to accelerate actin elongation, we tested if this effect depends on the vimentin concentration. To this end, we took advantage of the vimentin Y117L mutant, which allows for the precise control of both the number and oligomerization state of vimentin. Actin polymerization assays were performed with 0.5 µM ATP-G-actin in the presence of vimentin Y117L at concentrations ranging from 0 to 1.18 mg/mL. The elongation rate increased in a dose-dependent manner, saturating at relatively low vimentin concentrations (Fig. 2D). The maximal effect corresponded to a ~28% increase in elongation rate, and half-maximal acceleration was reached at ~0.13 mg/mL vimentin Y117L. Hence, the promoting effect of vimentin on actin elongation reaches saturation with

only a limited amount of vimentin, as compared to the physiological range (estimated to be > 1 mg/mL in Hela cells (42)).

Vimentin promotes actin elongation by preventing the departure of monomers

The net elongation rate of actin filaments at the barbed end reflects the result of actin monomer association and dissociation events. To gain insights into the mechanism by which vimentin accelerates actin elongation, we sought to determine how the arrival and the departure of monomers at the barbed end were respectively affected by vimentin. To do so, we repeated the actin polymerization assay at different ATP-G-actin concentrations (Fig. 3A). The elongation rates displayed an affine relationship with the ATP-G-actin concentration, allowing the extraction of the on-rate (slope) and the off-rate (intercept), called k_{on}^{ATP} and k_{off}^{ATP} respectively. Strikingly, we observed that vimentin reduced the actin off-rate close to zero, while having no significant effect on the on-rate (Fig. 3B). Thus, vimentin accelerates actin elongation by stabilizing monomers at the growing barbed end rather than increasing the monomer binding rate (Fig. 3C). This potentially explains the saturating dose-dependence, since the off-rate cannot be further reduced below zero.

Vimentin does not stabilize actin filaments against depolymerization

The stabilization of ATP-actin subunits at the barbed end induced by vimentin during polymerization led us to test whether vimentin could also protect actin filaments from depolymerization. We performed an actin depolymerization assay where non-biotinylated actin filaments were first polymerized from spectrin-actin seeds. Then, unpolymerized actin monomers were washed out, and filament depolymerization was monitored using methylcellulose to keep the filaments close to the surface (Fig. 3D). We observed no significant effect of vimentin on the depolymerization rate, indicating that vimentin stabilizes the barbed end only when the actin filament is growing (Fig. 3D). This surprising result might be explained by the difference in state of the barbed end under polymerizing and depolymerizing conditions. Upon incorporation into a filament, the conformational change of the subunits triggers the ATP hydrolysis to ADP.Pi within seconds, and the inorganic phosphate is then released with a half-time of a few minutes (43–45). Actin subunits can thus exist under three different nucleotide states (ATP-, ADP.Pi- and ADP-actin). In polymerizing conditions, as soon as the polymerization rate is faster than the ATP hydrolysis rate (0.3 s^{-1} (46)), the barbed end is occupied by ATP-actin subunits, and the off-rate measured indirectly corresponds to the dissociation of ATP-actin subunits (k_{off}^{ATP}, Fig. 3C). In contrast, in the depolymerization assay, we monitor the disassembly of ADP/ADP.Pi actin subunits ($k_{off}^{ADP/ADP.Pi}$, Fig. 3D). Note that we do not monitor the depolymerization of fully ADP-actin filaments, as the buffer contains 1 mM sodium phosphate, which comes with vimentin, preventing the full conversion to ADP-actin filaments by maintaining an equilibrium between filament-bound and soluble phosphate (see Methods). The fact that vimentin has no impact on ADP/ADP.Pi depolymerization suggests that its stabilizing action at the barbed end is specific to ATP-actin subunits.

Vimentin stabilizes ATP-actin, but not ADP-actin monomers at the barbed end

To assess the influence of the actin nucleotide state on the stabilizing effect of vimentin, we monitored actin polymerization from ADP-actin monomers (ADP-G-actin) by converting ATP-G-actin into ADP-G-actin prior to the assay (Fig. 3E). Because ADP-actin has a higher critical concentration than ATP-actin (43, 47, 48), we performed the actin polymerization assay at 4 µM ADP-G-actin instead of 0.5 µM, and in a Tris buffer without phosphate to avoid any conversion to ADP.Pi. However, this higher actin concentration increased the background signal when a small fraction of actin was fluorescently labeled, preventing accurate tracking of filament elongation. To overcome this constraint, we used a low concentration (50 nM) of a fluorescently labeled actin filament–binding domain from utrophin, which reliably reports filament length without interfering with assembly (49, 50) or with the effect of vimentin on actin elongation (Fig. S4). Unlike with ATP-actin, we did not observe any acceleration of ADP-actin polymerization by vimentin, indicating that the stabilizing effect of vimentin depends on the nucleotide state of the actin subunits and occurs only for ATP-actin. Taken together, these results demonstrate that vimentin can stabilize the barbed end of actin filaments when occupied by ATP-actin subunits,

thereby enhancing polymerization. In contrast, when the barbed end is composed of ADP-actin subunits, as in depolymerizing filaments, vimentin has no stabilization effect, which explains the absence of effect on actin depolymerization.

Vimentin promotes actin nucleation

Vimentin's stabilizing effect on ATP-actin subunits at the barbed end significantly lowers the critical concentration for net ATP-actin elongation, defined as the ratio between the actin off-rate k_{off}^{ATP} and the on-rate k_{on}^{ATP}. We hypothesized that vimentin could also enhance the nucleation of actin filaments, which requires the formation of a critical nucleus, most commonly described as a tetramer (51), although some models suggest a trimer (52). Because the low oligomeric states are unstable, their formation represents the principal barrier to nucleation. By stabilizing the interaction between ATP-actin subunits, vimentin could reduce this barrier and promote actin oligomerization to form a critical nucleus. To test this hypothesis, we first analyzed the ability of vimentin to nucleate actin filaments in bulk using a pyrene fluorescence assay (Fig. 4A). The presence of vimentin decreased the initial lag time associated with actin filament nucleation, and fitting the curves using the off-rate k_{off}^{ATP} and on-rate k_{on}^{ATP} values extracted from previous experiments (Fig.3) revealed a ~50% increase in the initial nucleation rate (Fig. 4B). The differences in plateau intensity were also consistent with the difference in critical elongation concentration we characterized. Then, we designed a fluorescence microscopy assay to directly visualize the nucleation of actin filaments. We mixed ATP-G-actin at low concentration (300 nM, 10% fluorescently labeled) in assembly buffer without or with pre-formed vimentin filaments, and confined the sample between two passivated glass coverslips, allowing us to detect and count filaments over time (Fig. 4C). We observed that the addition of vimentin filaments increased the number of actin filaments created by unit of time (Fig. 4D). Taken together, these results show that vimentin, beyond lowering the actin critical concentration for elongation, also accelerates the earliest steps of filament formation, providing a direct mechanism by which vimentin intermediate filaments can modulate actin network assembly.

Vimentin interacts directly and weakly with actin monomers

The effect of vimentin on actin nucleation suggests the existence of a direct interaction between vimentin and actin monomers. To test this, we designed a pull-down assay in which varying amounts of vimentin filaments were immobilized on magnetic beads and used to capture interacting ATP-G-actin (Fig. 5A). Pellets and supernatants were analyzed by SDS-PAGE followed by gel staining, with known concentrations of actin and vimentin loaded on the same gel to generate calibration curves (Fig. 5B). We observed that the fraction of actin recovered in the pellet increased with the amount of vimentin on the beads (Fig. 5C). Assuming that the assay probes the "binding" regime, where vimentin is present in excess relative to actin (53) and considering a simple reaction with a 1:1 stoichiometry between actin and vimentin monomers, we fitted the fraction of actin specifically bound to the vimentin-coated beads (*F*) as a function of the free vimentin concentration in the pellet (C_{vim}^{free}) with the equation: $F = 1/(1 + K_D/C_{vim}^{free})$, where K_D is the actin-vimentin dissociation constant (Fig. 5D). Pooling the data from 5 independent experiments allowed us to estimate K_D to be of the order of 10 µM, consistent with a weak interaction. This value should be considered approximate. First, actin in solution may not be strictly monomeric due to spontaneous nucleation, potentially leading to an underestimation of the dissociation constant. Second, although our quantification method accounts for the non-specific binding of actin to the beads, such binding may be reduced when beads are coated with vimentin, which would instead lead to an overestimation of the dissociation constant. Finally, the 1:1 stoichiometry hypothesis is a strong assumption. Vimentin could have several actin-binding sites, leading to an underestimation of the dissociation constant. Conversely, all vimentin binding sites might not be accessible, leading to an overestimation of the dissociation constant. Despite these limitations, our data provide strong evidence for a direct and specific interaction between vimentin and actin monomers.

Discussion

In this work, we addressed the question of the direct interaction between actin and vimentin at the molecular level, providing new insight into cytoskeletal crosstalk. Using in vitro assays, we found that the sole presence of vimentin enhances actin nucleation and barbed-end elongation by specifically stabilizing ATP-actin subunits, without interfering with the addition of additional monomers. Pull-down experiments confirmed a weak but direct interaction between the two proteins. Together, our findings identify vimentin as an unexpected regulator of actin dynamics and highlight a novel mechanism by which intermediate filaments can directly influence actin networks.

Our results rule out macromolecular crowding as an explanation of vimentin's effect on actin dynamics. Previous in vitro studies using inert macromolecules have shown that macromolecular crowding can accelerate actin elongation, most likely due to excluded volume effects (54, 55). However, this effect requires concentrations of crowders typically above 20 mg/mL, a range we verified in our experimental conditions using Dextran (54)(Fig. S5A). At 20 mg/mL, the volume occupied by Dextran macromolecules (40 kDa) can be estimated to be around 15%, assuming spheres with a hydrodynamic radius of 5 nm (56). In contrast, the accelerating effect of vimentin occurs at much lower concentrations (~0.2 mg/mL) and quickly saturates at higher vimentin concentrations (~1 mg/mL). In this range, the volume excluded by vimentin remains negligible (<0.5%) and cannot account for the observed acceleration. Moreover, the mechanism we uncovered – stabilization of ATP-actin at the barbed end through a decrease in the off-rate while leaving the on-rate unaffected – is fundamentally different from the effect of inert crowders. Indeed, these crowders accelerate elongation by increasing the on-rate, which can be interpreted as an increase in the effective monomer concentration (55)(Fig. S5B). Finally, if excluded volume effects had a significant role in vimentin's effect, one would expect vimentin's effect to be independent of actin nucleotide state, and to observe the same acceleration for ADP-actin polymerization, which we did not observe. Altogether, these three observations - the low vimentin concentrations at which its effect occurs, the demonstrated stabilizing mechanism, and the dependency on actin nucleotide state - argue strongly against a role of crowding.

The specific stabilization of ATP-actin but not ADP-actin subunits at filament barbed ends by vimentin is an intriguing result. One possible explanation for this nucleotide dependence could be a difference in the accessibility of actin residues which can interact with vimentin. So far, only the structure of the barbed end with a terminal actin subunit in the ADP-state, which is in an F-actin conformation, has been obtained (57, 58). One can speculate that, during elongation, the recently added terminal subunit in the ATP-state could transiently remain in a G-actin-like conformation, which could thus allow it to interact with vimentin as shown by our pull-down assay.

The domain(s) of vimentin implicated in its effect on actin elongation remain unknown, although we ruled out the implication of vimentin head and tail domains in the experiments using truncated constructs. Mapping the potential interaction sites, for example, by systematic point mutation within the rod domain, crosslinking, or using structural approaches, would be critical to understand the actin-vimentin binding interface and how vimentin specifically stabilizes ATP-actin at the barbed end. Cryogenic electron microscopy has been instrumental in understanding the mechanisms involved in actin assembly (59, 45, 58) and how it is regulated by actin-binding proteins at the barbed end (57, 60–62). Similar high-resolution structural approaches applied to F-actin and vimentin are required to reveal whether vimentin directly contacts actin subunits at the barbed end or indirectly modulates their conformation.

The interaction between vimentin and actin is expected to be weak and transient. Pull-down experiments yielded an estimated dissociation constant of ~10 µM, corresponding to the ratio of the off-rate to the on-rate of the actin-vimentin interaction. Given that vimentin is expected to associate with the growing barbed end at elongation rates as high as 20 subunits/s at 1 mg/mL vimentin (18 µM monomers), it suggests that the on-rate of vimentin on actin subunits of the barbed end should be higher than ~10^6 $M^{-1}.s^{-1}$. From the dissociation constant, the corresponding off-rate could be estimated > 10 s^{-}

[1], which is consistent with the fact that we could not observe the recruitment of actin monomers on vimentin filaments in our fluorescence assay with limited time resolution (37). We therefore propose that frequent but transient interactions of vimentin in the vicinity of the barbed end of actin filaments underlie the stabilizing effect that we have characterized. Nevertheless, we do not resolve the precise interaction, and it is not possible to count how many actin subunits from the barbed end are interacting with vimentin subunits. Multiple bonds may exist with some level of cooperativity between them, making a precise kinetic model difficult to assess. Interestingly, recent in vitro studies on microtubules demonstrated that vimentin stabilizes dynamic microtubules (63). Similar to the actin-vimentin interaction described here, the microtubule-vimentin interaction is weak and transient, but sufficient to have a stabilization effect on microtubule dynamics without inducing co-alignment or bundling between the two filament types. In contrast to its effect on actin, vimentin does not increase microtubule elongation rate, but instead decreases the catastrophe frequency and increases the rescue frequency. The differences between vimentin's effect on microtubules and on actin may arise from their distinct architectures and assembly pathways, although the underlying molecular mechanisms could be similar. However, because the study of the dynamic instability requires microtubules assembled from GTP-tubulin, the dependence of vimentin's effect on the tubulin nucleotide state could not be directly assessed. Together, these findings suggest that vimentin may act as a broad modulator of cytoskeletal turnover.

Vimentin differs from canonical actin barbed end regulators such as formins and Ena/VASP. These actin-binding proteins promote actin elongation through enhanced recruitment of (profilin-)actin monomers, thus having a major impact on the apparent actin on-rate (64–66). In contrast, vimentin does not increase the recruitment of monomers but instead stabilizes the barbed end. This suggests that vimentin does not act as a dominant driver of actin polymerization, such as formin and Ena/VASP, but may rather provide a layer of fine-tuning that contributes to cytoskeletal remodeling in regions where vimentin, actin filaments, and regulatory factors converge. An intriguing possibility is that the effect of vimentin on the barbed end elongation might modify the activity of actin-binding proteins. Future work should test whether vimentin synergizes or competes with other actin regulators and how cross-linkers or signaling pathways could further tune this effect in cells.

Materials and Methods

Detailed protocols are included in the SI Appendix. We purified recombinant wild-type human vimentin and vimentin mutants from E. coli (8, 9, 37). Vimentin, stored in 8M urea at -70 °C, was renatured by stepwise dialysis to sodium phosphate buffer (pH 7.0, 2.5mM sodium phosphate, 1 mM DTT) then prepared in a buffer compatible with actin assembly (assembly buffer: 10 mM HEPES pH 7.0, 1 mM sodium phosphate, 1 mM $MgCl_2$, 0.2 mM EGTA, 100 mM KCl). KCl was added at the last minute to start filament assembly, using the so-called kick-start method. The vimentin mix, typically at 1 mg/mL, was then incubated at 37°C for 30 minutes. We followed the same steps for experiments with vimentin Y117L and vimentin Δhead. The assembly protocol had to be optimized for vimentin Δtail to prevent the formation of unexpected aggregates. Vimentin Δtail filaments were assembled in a modified assembly buffer (10 mM HEPES, pH 7.0, 1 mM sodium phosphate, 1 mM DTT, 0.2 mM EGTA, 50 mM KCl), supplemented with 1 mM $MgCl_2$ just before introducing the sample into the flow chamber. For ADP-actin polymerization experiments in Tris buffer, vimentin dialysed in Tris dialysis buffer (5 mM Tris-HCl pH 8.0, 1 mM DTT) was prepared in Tris assembly buffer (10 mM Tris-HCl, pH 7.0, 1 mM $MgCl_2$, 0.2 mM EGTA, 50 mM KCl). The vimentin mix was then incubated at 37°C for 1 h.

Alpha skeletal actin was purified from rabbit muscle and stored in G-buffer (2 mM Tris-HCl, pH 7.8, 1 mM DTT, 0.2 mM $CaCl_2$, 0.2 mM ATP, 0.01% NaN_3)(37, 44). Actin was labeled with Alexa Fluor (AF)-488, Atto-643 or Atto-488 NHS Ester.

Polymerization and depolymerization experiments in TIRF microscopy were performed in flow chambers made of two cleaned glass coverslips (22 x 40 mm, #1.5, VWR) silanized with dichlorodimethylsilane. The flow chamber was first coated with neutrAvidin at 10 µg/mL for 5 minutes and rinsed with assembly buffer. The surfaces were then passivated by incubation of Pluronic F127 1% for 15 min, thoroughly rinsed with the assembly buffer, and further passivated with bovine serum albumin (BSA) at 10 mg/mL for 5 min. Both F127 and BSA solutions were diluted in the assembly buffer. Biotinylated F-actin fragments were prepared by pre-assembly of F-actin (10% Atto-643-labeled, 10% biotinylated) in a test tube at 10 µM for 1 hour at room temperature (in G-buffer supplemented with 100 mM KCl), followed by a 1:500 dilution in assembly buffer containing Atto-643-labeled ATP-G-actin (non-biotinylated) at 0.2 µM to prevent depolymerization. The actin filaments were finally fragmented by strong pipetting and introduced into the flow chamber for a few seconds. The chamber was rinsed with the assembly buffer containing 0.2 µM Atto-643-labeled ATP-G-actin to remove unbound filaments. The polymerization experiment was then started by flowing 10 % AF 488 or Atto 488-labeled, 0.15 % biotinylated ATP-G-actin in assembly buffer (except for ADP-G-actin polymerization) supplemented with 0.2 mM ATP, as well as 1 mM DTT, 1.2 mg/mL glucose, 40 µg/mL glucose oxidase, and 8 µg/mL catalase used as oxygen scavengers to limit photobleaching and creation of reactive oxygen species. The ADP-G-actin polymerization assay was performed in the Tris assembly buffer, supplemented with 1 mM DTT and the oxygen scavengers. Observations were carried out on an inverted microscope (Nikon Eclipse Ti), using TIRF or wide field microscopy with a 60X objective NA 1.49. Images were acquired by a Kinetix camera (Teledyne Photometrics). The experiment was controlled using MicroManager. Movies were analyzed using TSOAX (67).

Acknowledgements

We thank the Romet-Lemonne/Jegou lab for assistance and exciting discussions and Ingrid Billaut-Chaumartin for careful reading of the manuscript. We thank Sarah Köster and Peter Bieling for sharing plasmids. CL thank Harald Herrmann and Tatjana Wedig for teaching her vimentin purification, and the support of the EU-supported Cooperation in Science and Technology (COST) action NANONET. This project was funded by “Investissements d’Avenir” Labex WhoAmI? (ANR-11-LABX-0071) and the Université Paris Cité IdEx (ANR-IDEX-0001), the Agence Nationale pour la recherche (ANR-21-CE11-0004-02), the Impulscience program of Fondation Bettencourt-Schueller and the Centre National de la Recherche Scientifique. LP was funded by La Ligue contre le Cancer (LNCC 282810).

References

1. J. E. Eriksson, *et al.*, Introducing intermediate filaments: from discovery to disease. *J. Clin. Invest.* **119**, 1763–1771 (2009).
2. C. Leduc, S. Etienne-Manneville, Intermediate filaments in cell migration and invasion: the unusual suspects. *Curr. Opin. Cell Biol.* **32**, 102–112 (2015).
3. H. Herrmann, U. Aebi, Intermediate Filaments: Structure and Assembly. *Cold Spring Harb. Perspect. Biol.* **8**, a018242 (2016).
4. S. Etienne-Manneville, Cytoplasmic intermediate filaments in cell biology. *Annu Rev Cell Dev Biol* **34**, 1–28 (2018).
5. R. A. Battaglia, S. Delic, H. Herrmann, N. T. Snider, Vimentin on the move: new developments in cell migration. [Preprint] (2018). Available at: https://f1000research.com/articles/7-1796 [Accessed 24 October 2025].
6. K. M. Ridge, J. E. Eriksson, M. Pekny, R. D. Goldman, Roles of vimentin in health and disease. *Genes Dev* **36**, 391–407 (2022).
7. C. Hookway, *et al.*, Microtubule-dependent transport and dynamics of vimentin intermediate filaments. *Mol Biol Cell* **26**, 1675–1686 (2015).
8. Q. D. Tran, *et al.*, Continuous self-repair protects vimentin intermediate filaments from fragmentation. *Proc. Natl. Acad. Sci.* **122**, e2417660122 (2025).
9. Q. D. Tran, V. Sorichetti, G. Pehau-Arnaudet, M. Lenz, C. Leduc, Fragmentation and Entanglement Limit Vimentin Intermediate Filament Assembly. *Phys. Rev. X* **13**, 011014 (2023).
10. F. Alisafaei, *et al.*, Vimentin is a key regulator of cell mechanosensing through opposite actions on actomyosin and microtubule networks. *Commun. Biol.* **7**, 658 (2024).
11. S. Duarte, *et al.*, Vimentin filaments interact with the actin cortex in mitosis allowing normal cell division. *Nat Commun* **10**, 1–19 (2019).
12. B. Eckes, *et al.*, Impaired mechanical stability, migration and contractile capacity in vimentin deficient fibroblasts. *J. Cell Sci.* **111**, 1897–1907 (1998).
13. M. P. Serres, *et al.*, F-actin interactome reveals vimentin as a key regulator of actin organization and cell mechanics in mitosis. *Dev Cell* **52**, 210–222 (2020).
14. F. Huber, A. Boire, M. P. López, G. H. Koenderink, Cytoskeletal crosstalk: when three different personalities team up. *Curr. Opin. Cell Biol.* **32**, 39–47 (2015).
15. S. Seetharaman, S. Etienne-Manneville, Cytoskeletal Crosstalk in Cell Migration. *Trends Cell Biol* **30**, 720–735 (2020).
16. L. Pradeau-Phélut, S. Etienne-Manneville, Cytoskeletal crosstalk: A focus on intermediate filaments. *Curr. Opin. Cell Biol.* **87**, 102325 (2024).
17. E. J. van Bodegraven, S. Etienne-Manneville, Intermediate filaments against actomyosin: the david and goliath of cell migration. *Curr Opin Cell Biol* **66**, 79–88 (2020).
18. Y. Jiu, *et al.*, Bidirectional Interplay between Vimentin Intermediate Filaments and Contractile Actin Stress Fibers. *Cell Rep.* **11**, 1511–1518 (2015).
19. Y. Jiu, *et al.*, Vimentin intermediate filaments control actin stress fiber assembly through GEF-H1 and RhoA. *J. Cell Sci.* **130**, 892–902 (2017).
20. X. Huang, *et al.*, Vimentin intermediate filaments coordinate actin stress fibers and podosomes to determine the extracellular matrix degradation by macrophages. *Dev. Cell* **60**, 1669-1685.e6 (2025).
21. N. Costigliola, *et al.*, Vimentin fibers orient traction stress. *Proc. Natl. Acad. Sci.* **114**, 5195–5200 (2017).
22. J. P. Conboy, M. G. Lettinga, P. E. Boukany, F. C. MacKintosh, G. H. Koenderink, Actin and vimentin jointly control cell viscoelasticity and compression stiffening. [Preprint] (2025). Available at: http://biorxiv.org/lookup/doi/10.1101/2025.01.01.630993 [Accessed 10 October 2025].
23. J. Hu, *et al.*, High stretchability, strength, and toughness of living cells enabled by hyperelastic vimentin intermediate filaments. *Proc. Natl. Acad. Sci.* **116**, 17175–17180 (2019).
24. A. Basu, *et al.*, Vimentin undergoes liquid–liquid phase separation to form droplets which wet and stabilize actin fibers. *Proc. Natl. Acad. Sci.* **122**, e2418624122 (2025).
25. P. González-Jiménez, *et al.*, Vimentin single cysteine residue acts as a tunable sensor for network organization and as a key for actin remodeling in response to oxidants and electrophiles. *Redox Biol.* **64**, 102756 (2023).
26. H. Wu, *et al.*, Vimentin intermediate filaments and filamentous actin form unexpected interpenetrating networks that redefine the cell cortex. *Proc. Natl. Acad. Sci.* **119**, e2115217119 (2022).
27. P. J. Hollenbeck, A. D. Bershadsky, O. Y. Pletjushkina, I. S. Tint, J. M. Vasiliev, Intermediate

filament collapse is an ATP-dependent and actin-dependent process. *J Cell Sci* **92**, 621–631 (1989).
28. A. Robert, H. Herrmann, M. W. Davidson, V. I. Gelfand, Microtubule-dependent transport of vimentin filament precursors is regulated by actin and by the concerted action of Rho- and p21-activated kinases. *FASEB J.* **28**, 2879–2890 (2014).
29. C. Leduc, S. Etienne-Manneville, Regulation of microtubule-associated motors drives intermediate filament network polarization. *J Cell Biol* **216**, 1689–1703 (2017).
30. A. S. Menko, *et al.*, A central role for vimentin in regulating repair function during healing of the lens epithelium. *Mol. Biol. Cell* **25**, 776–790 (2014).
31. S. Osmanagic-Myers, *et al.*, Plectin reinforces vascular integrity by mediating crosstalk between the vimentin and the actin networks. *J. Cell Sci.* **128**, 4138–4150 (2015).
32. I. Correia, D. Chu, Y.-H. Chou, R. D. Goldman, P. Matsudaira, Integrating the Actin and Vimentin Cytoskeletons: Adhesion-Dependent Formation of Fimbrin–Vimentin Complexes in Macrophages. *J. Cell Biol.* **146**, 831–842 (1999).
33. H. Kim, *et al.*, Filamin A is required for vimentin-mediated cell adhesion and spreading. *Am. J. Physiol.-Cell Physiol.* **298**, C221–C236 (2010).
34. O. Esue, A. A. Carson, Y. Tseng, D. Wirtz, A direct interaction between actin and vimentin filaments mediated by the tail domain of vimentin. *J. Biol. Chem.* **281**, 30393–30399 (2006).
35. Y. Shen, *et al.*, Effects of vimentin intermediate filaments on the structure and dynamics of in vitro multicomponent interpenetrating cytoskeletal networks. *Phys Rev Lett* **127**, 108101 (2021).
36. T. Golde, *et al.*, Glassy dynamics in composite biopolymer networks. *Soft Matter* **14**, 7970–7978 (2018).
37. I. I. Petitjean, *et al.*, Reconstitution of cytolinker-mediated crosstalk between actin and vimentin. *Eur. J. Cell Biol.* **103**, 151403 (2024).
38. V. Prahlad, M. Yoon, R. D. Moir, R. D. Vale, R. D. Goldman, Rapid Movements of Vimentin on Microtubule Tracks: Kinesin-dependent Assembly of Intermediate Filament Networks. *J. Cell Biol.* **143**, 159–170 (1998).
39. P. Soellner, R. A. Quinlan, W. W. Franke, Identification of a distinct soluble subunit of an intermediate filament protein: tetrameric vimentin from living cells. *Proc Natl Acad Sci* **82**, 7929–7933 (1985).
40. H. Herrmann, *et al.*, Structure and Assembly Properties of the Intermediate Filament Protein Vimentin: The Role of its Head, Rod and Tail Domains. *J Mol Biol* **264**, 933–953 (1996).
41. M. Meier, *et al.*, Vimentin Coil 1A—A Molecular Switch Involved in the Initiation of Filament Elongation. *J. Mol. Biol.* **390**, 245–261 (2009).
42. D. B. Bekker-Jensen, *et al.*, An Optimized Shotgun Strategy for the Rapid Generation of Comprehensive Human Proteomes. *Cell Syst* **4**, 587-599.e4 (2017).
43. I. Fujiwara, D. Vavylonis, T. D. Pollard, Polymerization kinetics of ADP- and ADP-Pi-actin determined by fluorescence microscopy. *Proc. Natl. Acad. Sci.* **104**, 8827–8832 (2007).
44. A. Jégou, *et al.*, Individual actin filaments in a microfluidic flow reveal the mechanism of ATP hydrolysis and give insight into the properties of profilin. *PLoS Biol.* **9**, e1001161 (2011).
45. W. Oosterheert, B. U. Klink, A. Belyy, S. Pospich, S. Raunser, Structural basis of actin filament assembly and aging. *Nature* **611**, 374–379 (2022).
46. L. Blanchoin, T. D. Pollard, Hydrolysis of ATP by Polymerized Actin Depends on the Bound Divalent Cation but Not Profilin. *Biochemistry* **41**, 597–602 (2002).
47. R. Cooke, Role of the bound nucleotide in the polymerization of actin. *Biochemistry* **14**, 3250–3256 (1975).
48. T. D. Pollard, Polymerization of ADP-actin. *J. Cell Biol.* **99**, 769–777 (1984).
49. P. Bieling, *et al.*, WH2 and proline-rich domains of WASP-family proteins collaborate to accelerate actin filament elongation. *EMBO J.* **37**, 102–121 (2018).
50. J. Funk, *et al.*, Profilin and formin constitute a pacemaker system for robust actin filament growth. *eLife* **8**, e50963 (2019).
51. L. S. Tobacman, E. D. Korn, The kinetics of actin nucleation and polymerization. *J. Biol. Chem.* **258**, 3207–3214 (1983).
52. D. Sept, J. A. McCammon, Thermodynamics and Kinetics of Actin Filament Nucleation. *Biophys. J.* **81**, 667–674 (2001).
53. I. Jarmoskaite, I. AlSadhan, P. P. Vaidyanathan, D. Herschlag, How to measure and evaluate binding affinities. *eLife* **9**, e57264 (2020).
54. D. Drenckhahn, T. D. Pollard, Elongation of actin filaments is a diffusion-limited reaction at the barbed end and is accelerated by inert macromolecules. *J. Biol. Chem.* **261**, 12754–12758 (1986).

55. R. A. Lindner, G. B. Ralston, Macromolecular crowding: effects on actin polymerisation. *Biophys. Chem.* **66**, 57–66 (1997).
56. J. K. Armstrong, R. B. Wenby, H. J. Meiselman, T. C. Fisher, The Hydrodynamic Radii of Macromolecules and Their Effect on Red Blood Cell Aggregation. *Biophys. J.* **87**, 4259–4270 (2004).
57. P. J. Carman, K. R. Barrie, G. Rebowski, R. Dominguez, Structures of the free and capped ends of the actin filament. *Science* **380**, 1287–1292 (2023).
58. W. Oosterheert, *et al.*, Molecular mechanisms of inorganic-phosphate release from the core and barbed end of actin filaments. *Nat. Struct. Mol. Biol.* **30**, 1774–1785 (2023).
59. S. Z. Chou, T. D. Pollard, Mechanism of actin polymerization revealed by cryo-EM structures of actin filaments with three different bound nucleotides. *Proc. Natl. Acad. Sci.* **116**, 4265–4274 (2019).
60. W. Oosterheert, *et al.*, Molecular mechanism of actin filament elongation by formins. *Science* **384**, eadn9560 (2024).
61. J. Funk, *et al.*, A barbed end interference mechanism reveals how capping protein promotes nucleation in branched actin networks. *Nat. Commun.* **12**, 5329 (2021).
62. N. J. Palmer, K. R. Barrie, R. Dominguez, Mechanisms of actin filament severing and elongation by formins. *Nature* **632**, 437–442 (2024).
63. L. Schaedel, C. Lorenz, A. V. Schepers, S. Klumpp, S. Köster, Vimentin intermediate filaments stabilize dynamic microtubules by direct interactions. *Nat Commun* **12**, 3799 (2021).
64. D. Breitsprecher, *et al.*, Molecular mechanism of Ena/VASP-mediated actin-filament elongation. *EMBO J.* **30**, 456–467 (2011).
65. N. Courtemanche, J. L. Henty-Ridilla, Actin filament dynamics at barbed ends: New structures, new insights. *Curr. Opin. Cell Biol.* **90**, 102419 (2024).
66. S. Romero, *et al.*, Formin is a processive motor that requires profilin to accelerate actin assembly and associated ATP hydrolysis. *Cell* **119**, 419–429 (2004).
67. T. Xu, *et al.*, Automated Tracking of Biopolymer Growth and Network Deformation with TSOAX. *Sci. Rep.* **9**, 1717 (2019).
68. L. K. Doolittle, M. K. Rosen, S. B. Padrick, “Measurement and Analysis of In Vitro Actin Polymerization” in *Adhesion Protein Protocols*, A. S. Coutts, Ed. (Humana Press, 2013), pp. 273–293.

Figures

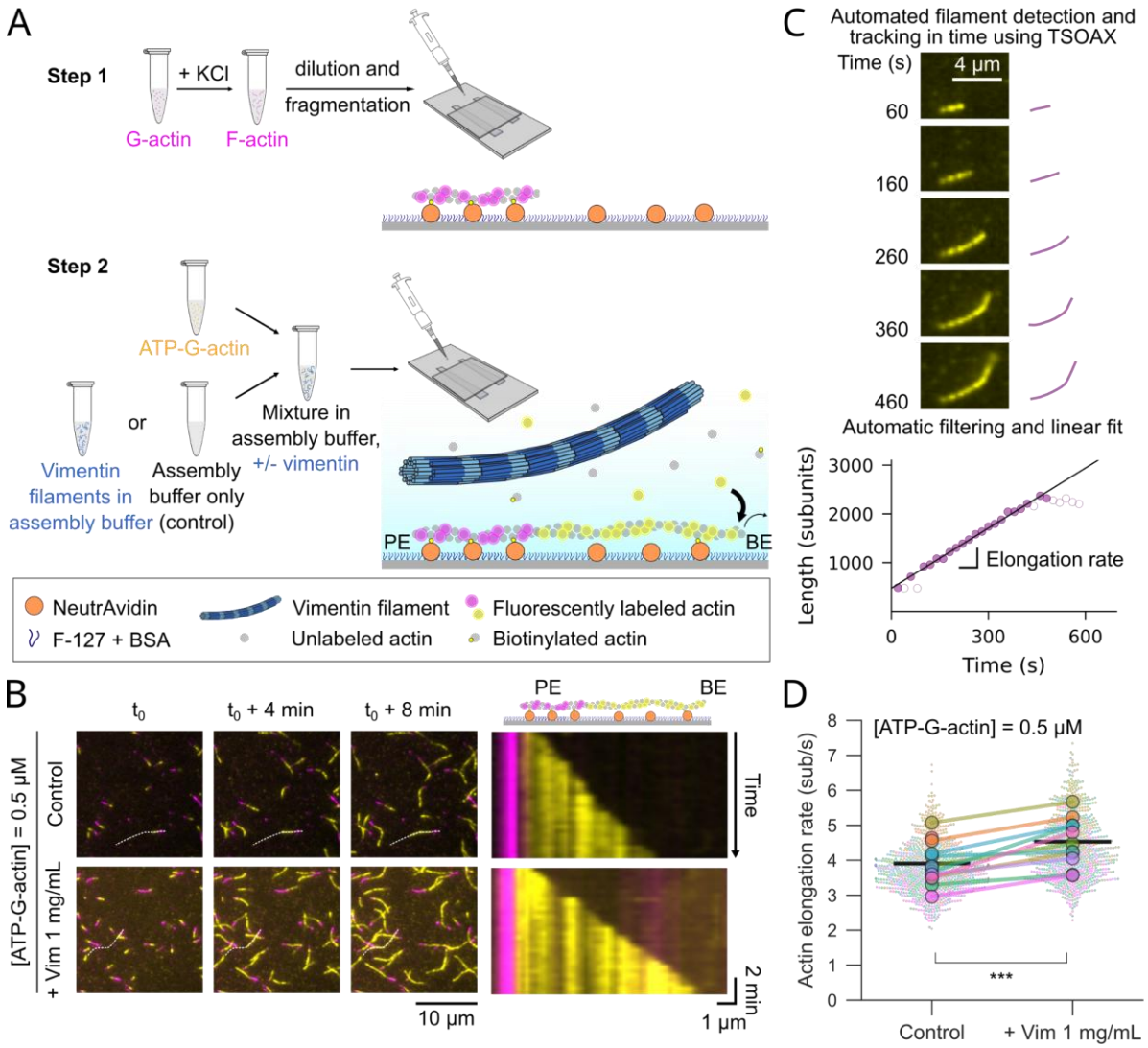

Figure 1: Vimentin promotes actin filament elongation at the barbed end

A) Actin polymerization assay. Step 1: Fragments of actin filaments (10% Atto-643, 10% biotin labeled, magenta) were pre-polymerized for ≥1h at 10 µM by adding 100 mM KCl to the ATP-G-actin solution in G-buffer, then diluted and fragmented by pipetting and introduced in a flow chamber that was functionalized with neutrAvidin and passivated by F127 and BSA. Step 2: ATP-G-actin (10% AF-488 or Atto-488, 0.15% biotin labeled, yellow) was mixed at a concentration of 0.5 µM in assembly buffer (10 mM HEPES pH 7.0, 1 mM sodium phosphate, 1 mM $MgCl_2$, 0.2 mM EGTA, 100 mM KCl) only (Control) or in buffer with 1 mg/mL of pre-assembled unlabeled wild-type vimentin filaments. This solution was then introduced in the flow chamber, and actin monomers assembled from the barbed end of the anchored F-actin fragments in the presence or absence of vimentin (blue). Actin filament elongation was monitored by TIRF microscopy. PE: pointed end, BE: barbed end.

B) Left: representative TIRF snapshots of actin filaments polymerizing without (Control) or with (+ Vim 1 mg/mL) vimentin filaments. Right: representative kymographs of actin filaments elongating from their barbed end, corresponding to filaments marked by dashed lines on the snapshots.

C) Method used to quantify the actin elongation rate. Top: example of TIRF time-lapse sequence of an elongating filament, along with the corresponding segmentation by the software TSOAX (67). Bottom: length in subunits of this actin filament as a function of time. The elongation rate was quantified by automatic filtering of detection errors (open circles) and linear fitting. Detection errors are due to the sparse anchoring of the filament: between two anchoring points, the filament can sometimes grow out-of-plane, leading to a low TIRF signal and an underestimation of its length.

D) Actin elongation rate in the absence (Control) or in the presence (+ Vim 1 mg/mL) of vimentin filaments. Colors depict experiments performed on the same day. Small dots: individual actin filament elongation rates ($n \geq 20$ rates per experiment), large dots: average elongation rates of the replicates ($N = 11$ independent replicates), black bars: mean elongation rate computed from the replicate averages. Statistical significance of the difference was evaluated by running a two-tailed paired t-test over the replicate averages. ***, p<0.001.

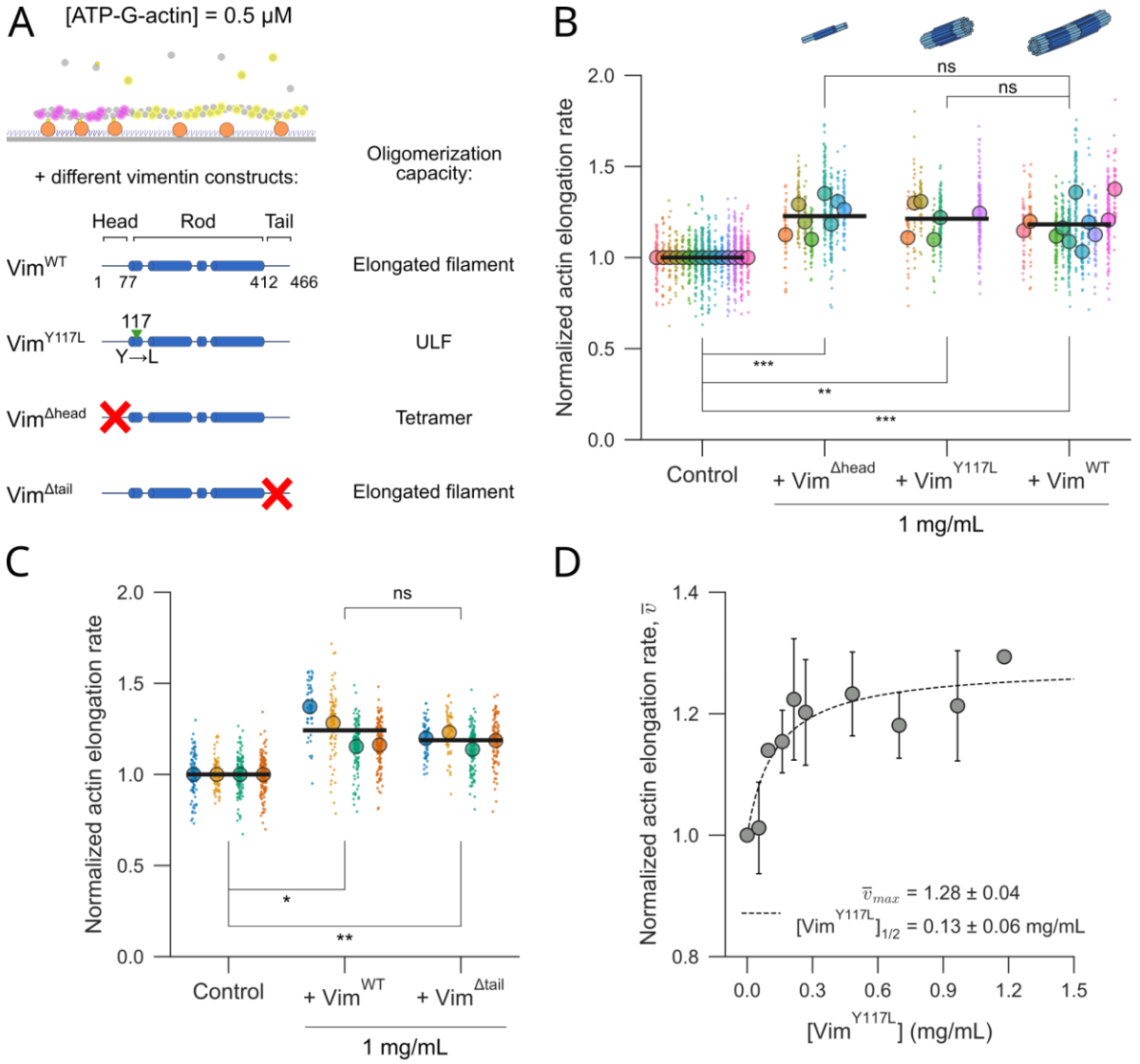

Figure 2: Vimentin acceleration of actin elongation is independent of its oligomerization state and tail domain, and is dose-dependent

A) The actin polymerization assay (at 0.5 μM ATP-G-actin, 10% labeled) was performed in the presence of different vimentin constructs. Wild-type vimentin (Vim^{WT}) and tailless vimentin ($Vim^{\Delta tail}$) assemble into filaments. Vim^{Y117L} assembles into ULFs that do not anneal end-to-end. Headless-vimentin ($Vim^{\Delta head}$) forms tetramers that do not assemble into filaments. The numbers represent the positions of the residues that delimit the head and tail domains.

B) Actin elongation rate in the absence (Control) or in the presence of 1 mg/mL vimentin (18 μM vimentin monomers) under different oligomerization states (+ $Vim^{\Delta head}$, Vim^{Y117L} or Vim^{WT}), normalized by the average rate of the control condition for each replicate. Colors depict experiments performed on the same day. Small dots: individual normalized actin filament elongation rates ($n \geq 20$ rates per replicate), large dots: average normalized elongation rates of the replicates ($Vim^{\Delta head}$: $N = 8$, $Vim^{\Delta head}$: $N = 6$, Vim^{WT}: $N = 11$ independent replicates), black bars: mean normalized elongation rate computed from the replicate averages. The data shown for wild-type vimentin are the same as shown in Fig. 1D.

C) Normalized actin elongation rate in the absence (Control) or in the presence of 1 mg/mL of Vim^{WT} or $Vim^{\Delta tail}$ filaments. Small dots: individual normalized actin filament elongation rates ($n \geq 20$ rates per replicate), large dots: average normalized elongation rates of the replicates ($N = 4$ independent replicates), black bars: mean normalized elongation rate computed from

the replicate averages. Experiments in C were conducted in the standard assembly buffer at 50 mM KCl. Statistical significance of the differences between conditions in B and C was evaluated by running two-tailed paired t-tests over the replicate averages. * p<0.05, ** p<0.01, *** p<0.001, ns: not significant (p>0.05).

D) Normalized actin elongation rate ($\underline{v}$) as a function of Vim^{Y117L} concentration ($[Vim^{Y117L}]$). Elongation rates were normalized by the average rate of the control condition (without Vim^{Y117L}) measured on the same day. Data are shown as the mean $\pm$ standard deviation of $1 \leq N \leq 8$ replicates. The mean normalized rates ($\underline{v}$) were fitted to the equation: $\underline{v} = 1 + (\underline{v}_{max} - 1)/(1 + [Vim^{Y117L}]_{1/2}/[Vim^{Y117L}])$ to extract the plateau value ($\underline{v}_{max}$, maximal normalized elongation rate in the presence of Vim^{Y117L}) and the Vim^{Y117L} concentration where half of the plateau is reached ($[Vim^{Y117L}]_{1/2}$). Error values on the estimated parameters represent the square root of the variances of the estimated parameters, extracted from the covariance matrix returned by the numpy.polyfit function in Python.

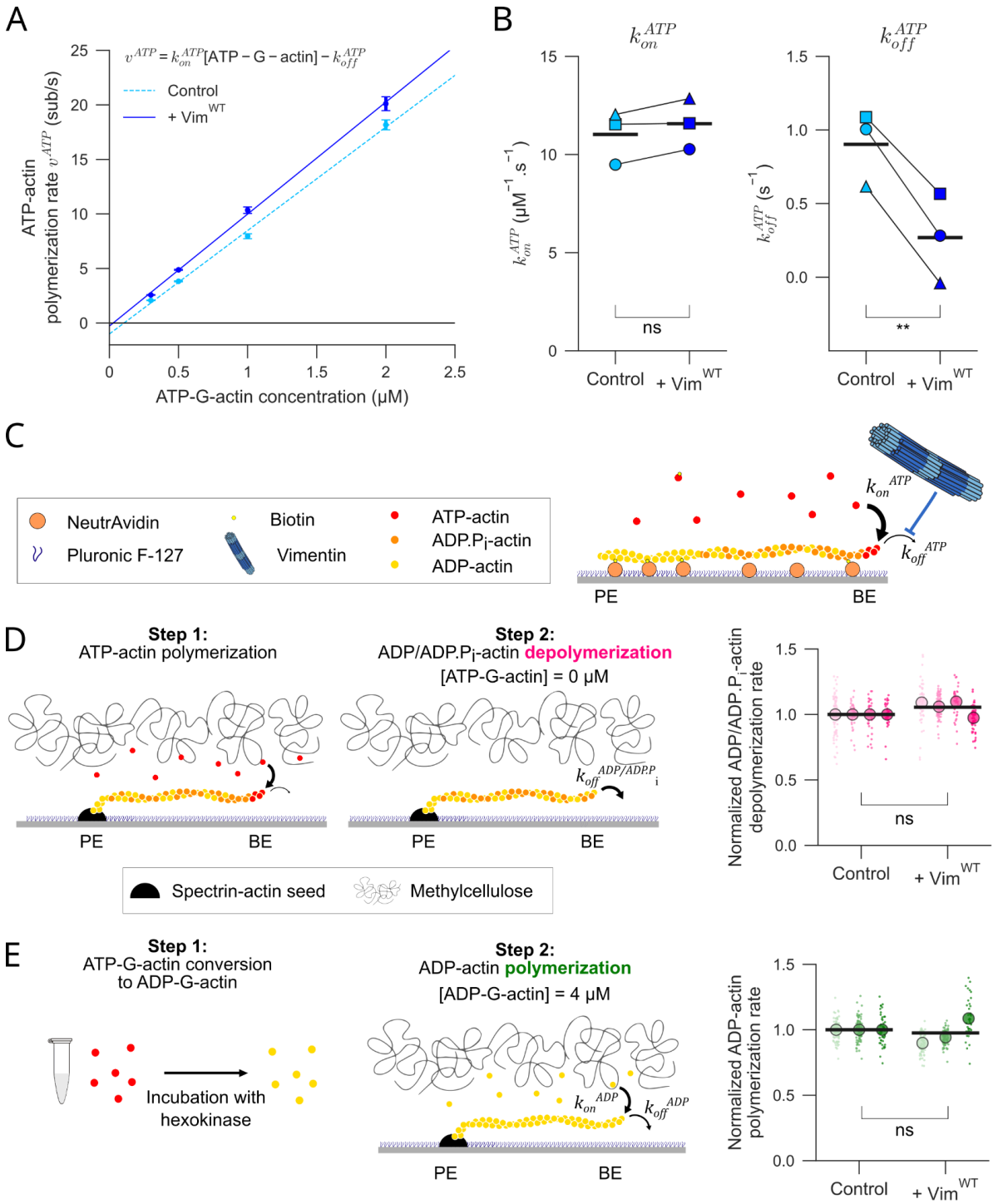

Figure 3: Vimentin decreases the off-rate of ATP-actin but not ADP-actin

A) Actin elongation rate as a function of ATP-G-actin concentration in the absence (Control, light blue) or in the presence of vimentin filaments at 1 mg/mL (+ Vim^{WT}, dark blue). Data are shown as the mean $\pm$ standard error of the mean for $n \geq 20$ rates per condition. Dashed and solid lines represent linear fits of the means to the equation above, to extract the on- and off-rates k_{on}^{ATP} and k_{off}^{ATP}. Experiments were conducted in the standard assembly buffer at 50 mM KCl.

B) Quantification of the ATP-actin on- and off-rates k_{on}^{ATP} and k_{off}^{ATP} extracted from $N = 3$ independent replicates (filled symbols) and mean rates (black bars), in the absence (Control, light blue) or in the presence of vimentin filaments (+Vim^{WT}, dark blue) at 1 mg/mL.

C) Schematics of the nucleotide states of actin in the standard actin polymerization assay. The barbed end (BE) is occupied by ATP-actin subunits (red), and free ATP-actin monomers in solution bind and unbind from the barbed end with rates k_{on}^{ATP} and k_{off}^{ATP}, respectively. Deeper within the filament, actin subunits exist as ADP.P_i-actin (orange) and ADP-actin (yellow). Vimentin (blue) increases the net ATP-actin elongation rate by decreasing the ATP-actin off-rate k_{off}^{ATP}.

D) Actin depolymerization assay. Step 1: actin filaments were polymerized from spectrin-actin seeds by flowing ATP-actin monomers in the flow chamber. Step 2: non-polymerized actin monomers were rinsed, and the depolymerization of actin filaments was monitored by TIRF microscopy, keeping the filaments close to the surface using methylcellulose. As the assembly buffer contains 1 mM sodium phosphate, the depolymerization rate results from the off-rates of both ADP.Pi- and ADP-actin. Right: normalized ADP/ADP.P_i-actin depolymerization rate in the absence (Control) or in the presence (+ Vim^{WT}) of vimentin filaments at 1 mg/mL. Small dots: individual normalized actin depolymerization rates ($n \geq 20$ rates per replicate), large dots: average normalized depolymerization rates of the replicates ($N = 4$ independent replicates), black bars: mean normalized depolymerization rate computed from the replicate averages.

E) ADP-actin polymerization assay. Step 1: ADP-G-actin was obtained by incubating ATP-actin at 10 µM in ATP-free G-buffer supplemented with 2.5 mM glucose, 0.2 mM EGTA, 20 µM $MgCl_2$ and 15 U/mL hexokinase for 18 h on ice. Step 2: unlabeled ADP-G-actin was mixed with 50 nM Alexa488-labeled actin-binding domain of utrophin in Tris assembly buffer (see Methods) and introduced in a flow chamber to polymerize from spectrin-actin seeds. The ADP-actin concentration was 4 µM. The filaments were kept close to the surface by methylcellulose and their elongation was followed by TIRF microscopy. Right: normalized ADP-actin polymerization rate in the absence (Control) or in the presence (+ Vim^{WT}) of vimentin filaments at 1 mg/mL. Small dots: individual normalized ADP-actin polymerization rates ($n \geq 20$ rates per replicate), large dots: average normalized polymerization rates of the replicates ($N = 3$ independent replicates), black bars: mean normalized depolymerization rate computed from the replicate averages.

Statistical significance of the differences between conditions in B, D and E was evaluated by running two-tailed paired t-tests over the replicate averages. ** $p<0.01$, ns: not significant ($p>0.05$).

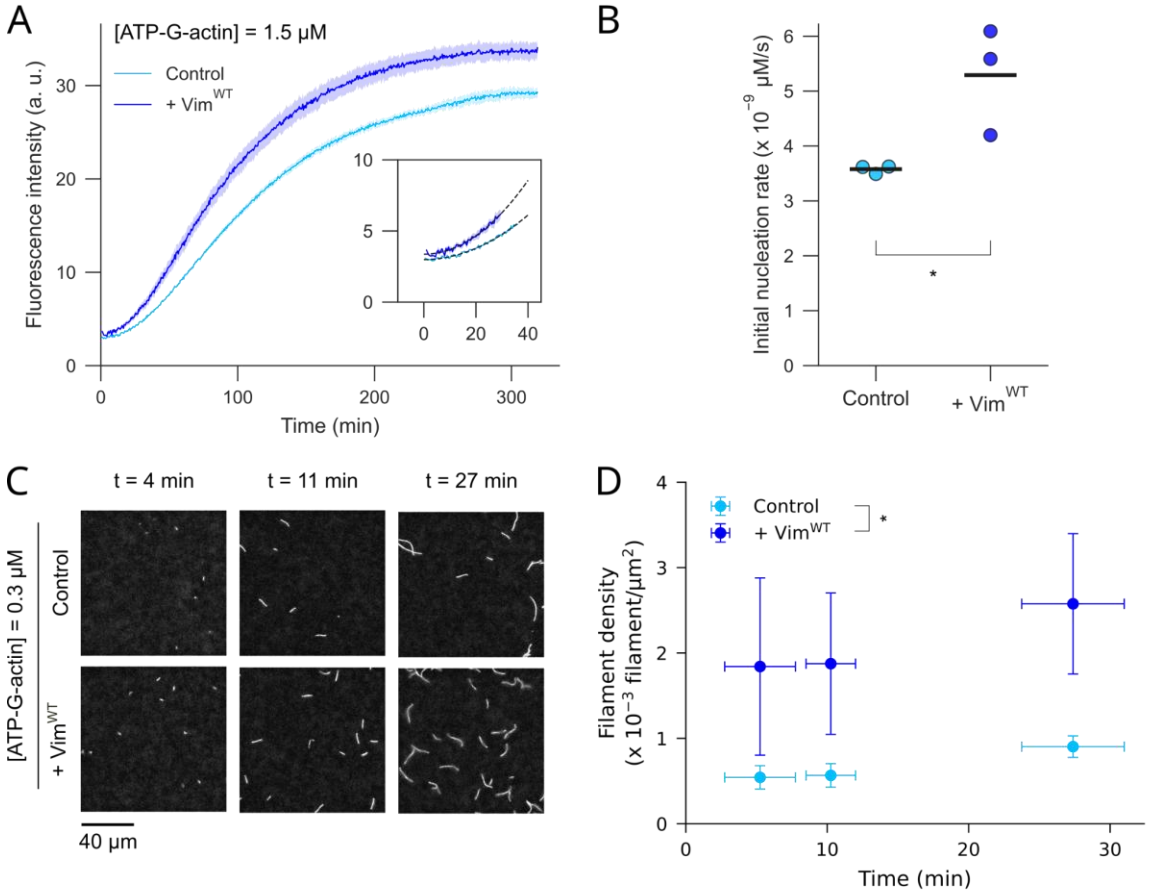

Figure 4: Vimentin promotes actin nucleation

A) Pyrene-actin fluorescence assay of actin assembly. Actin (1.5 µM, 8% pyrene-labeled) was assembled in the absence (Control, light blue) and in the presence of 1 mg/ml of pre-assembled wild-type vimentin filaments (+ Vim^{WT}, dark blue). The plain curves represent the means of N = 3 replicates, and the shaded regions the standard errors of the means. Raw fluorescence signals were corrected for the vimentin signal (see Methods). The inset shows an enlarged plot of the early time points used to fit the data (black dashed lines) following the method from Doolittle et al. (68) to extract the initial nucleation rate.

B) Quantification of the initial nucleation rate for the N = 3 replicates in A) in control (light blue) and vimentin (+ Vim^{WT}, dark blue) conditions. Dots: initial nucleation rates measured for each replicate, black bars: mean initial nucleation rates over the 3 replicates. Statistical significance of the difference between conditions was evaluated by running a two-tailed unpaired t-test. * $p<0.05$.

C) Direct visualization of actin nucleation by epifluorescence microscopy. Representative snapshots of nucleated actin filaments in the absence (Control) or in the presence of 1 mg/mL of pre-assembled wild-type vimentin filaments (+ Vim^{WT}). The ATP-G-actin concentration was 0.3 µM, with a 10% labeling fraction. Experiments were carried out in the standard assembly buffer, without adding methylcellulose. Instead, the samples were confined in thin chambers (height ~3 µm, see SI).

D) Quantification of the mean filament density in C) as a function of time in control (light blue) and vimentin (+ Vim^{WT}, dark blue) conditions. Each dot represents the mean +/- SEM of N = 4 replicates for a time interval depicted by the horizontal error bar. For each replicate, condition, and time point, the mean number of filaments from $24 \leq n \leq 94$ fields of view was computed. Statistical significance of the difference between conditions was evaluated by running a two-way ANOVA. * $p<0.05$.

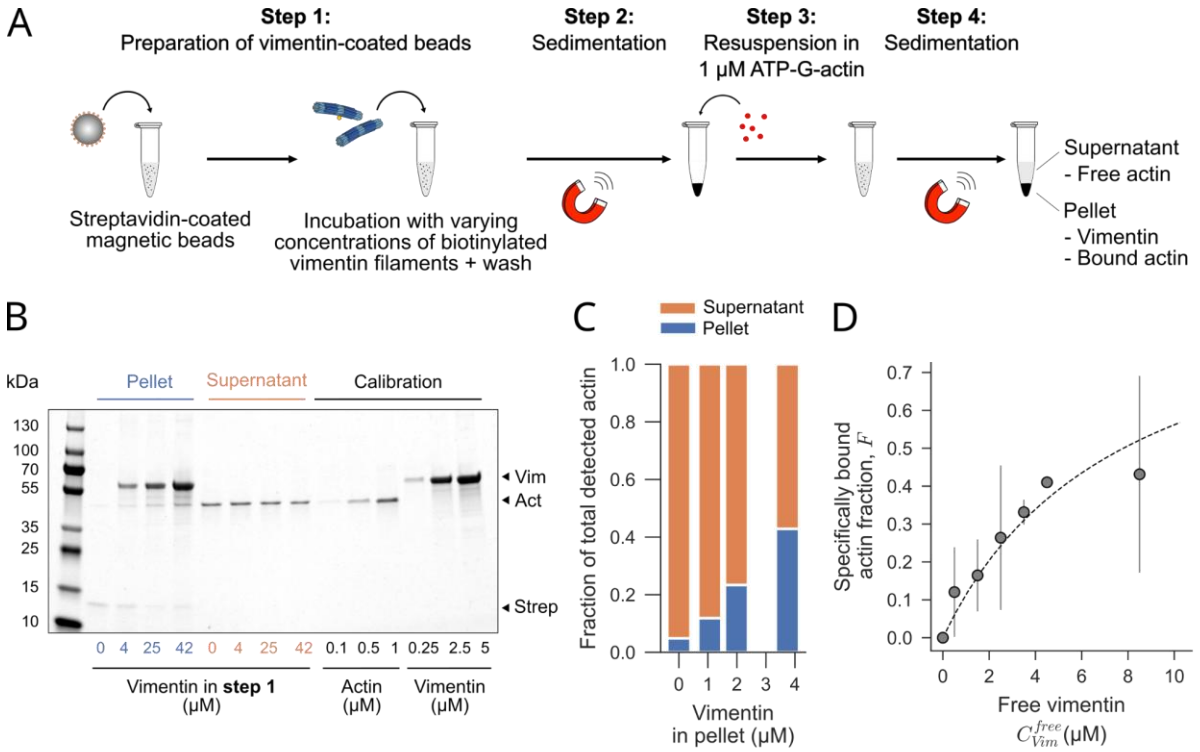

Figure 5: Vimentin directly interacts with actin

A) Actin-vimentin magnetic pull-down assay. In step 1, streptavidin-coated magnetic beads are incubated with varying concentrations of biotinylated vimentin filaments. In step 2, the beads are pulled with a magnet, and the supernatant containing unbound vimentin is discarded. The beads are further rinsed with buffer to completely remove unattached vimentin. In step 3, the vimentin-coated beads are resuspended in a solution containing 1 µM ATP-G-actin, and immediately pulled down with the magnet (step 4). The protein content of the pellet and the supernatant is then analyzed by SDS-PAGE. Step 3 and 4 were performed in less than a minute, limiting possible actin nucleation. The experiment was performed in the standard assembly buffer.

B) Representative SDS-PAGE gel obtained with the assay described in A. Four concentrations of vimentin ranging from 0 to 42 µM (in terms of vimentin monomers) were used in step 1, and for each concentration, the pellet and supernatant obtained after step 4 were loaded. The six lanes on the right were loaded with samples containing known concentrations of actin or vimentin for calibration. Arrowheads indicate bands corresponding to vimentin (Vim), actin (Act), and streptavidin (Strep). The streptavidin band intensity provides a readout of the magnetic bead concentration.

C) Quantification of the electrophoresis gel shown in B. Fraction of total detected actin found in the pellet (blue) and in the supernatant (orange) as a function of the vimentin concentration measured in the pellet.

D) Fraction of total actin in solution specifically pulled with vimentin *(F)*, as a function of the free vimentin concentration in the pellet (C_{vim}^{free}), expressed in µM of vimentin monomers. The amount of actin specifically bound to vimentin was estimated by subtracting the amount of actin non-specifically bound to the beads, and by taking into account the difference in bead concentration between conditions (see Methods). The free vimentin concentration is defined as the total vimentin concentration measured in the pellet, minus the concentration of vimentin bound to actin, which is equal to the concentration of bound actin, assuming a 1:1 stoechiometry. Data collected from N=5 independent experiments were pooled together, binned by C_{vim}^{free}, and are represented as the mean $\pm$ standard deviation. The data were fitted

(dashed line) to the equation: $F = 1/(1+K_D/C_{vim}^{free})$, where K_D, the only free parameter, provides an estimate for the actin-vimentin dissociation constant.